APL Materials

RESEARCH ARTICLE | DECEMBER 10 2018

Epitaxial lateral overgrowth of α-Ga_2O_3 by halide vapor phase epitaxy

Special Collection: Wide Bandgap Oxides

Y. Oshima; K. Kawara; T. Shinohe; T. Hitora; M. Kasu; S. Fujita

APL Mater. 7, 022503 (2019)
https://doi.org/10.1063/1.5051058

Epitaxial lateral overgrowth of α-Ga_2O_3 by halide vapor phase epitaxy

Cite as: APL Mater. 7, 022503 (2019); doi: 10.1063/1.5051058
Submitted: 6 August 2018 • Accepted: 11 September 2018 •
Published Online: 10 December 2018

Y. Oshima,[1,a)] K. Kawara,[2] T. Shinohe,[2] T. Hitora,[2] M. Kasu,[3] and S. Fujita[4]

AFFILIATIONS

[1] Optical Single Crystals Group, National Institute for Materials Science, 1-1 Namiki, 305-0044 Tsukuba, Japan
[2] FLOSFIA, Inc., Kyodai-Katsura Venture Plaza, 615-8245 Kyoto, Japan
[3] Department of Electrical and Electronic Engineering, Saga University, 1 Honjo-machi, 840-8502 Saga, Japan
[4] Department of Electronic Science and Engineering, Kyoto University, Katsura 615-8520, Kyoto, Japan

[a)] Author to whom correspondence should be addressed: OSHIMA.Yuichi@nims.go.jp

ABSTRACT

We demonstrate the epitaxial lateral overgrowth of α-Ga_2O_3 by halide vapor phase epitaxy. We prepared patterned SiO_2 masks on a (0001) α-Ga_2O_3/sapphire template, and then α-Ga_2O_3 islands were regrown selectively on the mask windows. The islands grew vertically and laterally to coalesce with each other. Facet control of the α-Ga_2O_3 islands was achieved by controlling the growth temperature, and inclined facets developed by decreasing the temperature. Transmission electron microscopy revealed that the crystal quality of the regrown α-Ga_2O_3 was improved owing to both the blocking of dislocations by the mask and the dislocation bending by the inclined facets.

Ga_2O_3 has been reported to possess five different polymorphs; these are the α-, β-, δ-, ε-, and γ-phases.[1] α-Ga_2O_3, the target material studied in the present work, is one of the metastable phases of Ga_2O_3 and crystalizes into the corundum structure. α-Ga_2O_3 is a wide bandgap semiconductor, and the bandgap energy has been reported to be 5.2–5.3 eV.[2,3] A high breakdown voltage and low on-resistance are expected because of the large bandgap energy, and therefore, α-Ga_2O_3 is promising for power device applications. Actually, Schottky barrier diodes with very low on-resistance beyond the SiC limit have already been demonstrated.[4] In addition, corundum-structured α-Ir_2O_3 and α-(Rh, Ga)$_2O_3$ have been shown to exhibit clear p-type conduction,[5,6] and therefore, bi-polar devices using the hetero-pn-junctions are expected.

In contrast to the case of thermodynamically stable β-Ga_2O_3, freestanding α-Ga_2O_3 wafers cannot be produced through the melt-growth technique. Accordingly, α-Ga_2O_3 films need to be grown by heteroepitaxy. The heteroepitaxy of α-Ga_2O_3 is possible on sapphire (α-Al_2O_3) substrates by mist-CVD[2] and halide vapor phase epitaxy (HVPE).[3] Although the crystal structures of α-Ga_2O_3 and sapphire both have the corundum structure, the lattice mismatch is large ($\Delta a/a \sim 4.5\%$, $\Delta c/c \sim 3.3\%$). Therefore, α-Ga_2O_3 epilayers usually include a high density of dislocations. Figure 1(a) shows a cross-sectional TEM image of a conventional α-Ga_2O_3 film grown on a (0001) sapphire substrate by HVPE. We can see a high density of dislocations propagating along the film growth direction. The dislocation density was estimated to be on the order of 10^{10} cm^{-2} from a plan-view TEM image of the same sample [Fig. 1(b)]. The crystal quality should be improved since such crystal defects could deteriorate the performance of α-Ga_2O_3 devices, although the influence of the defects has not yet been clarified.

To improve the crystal quality of heteroepitaxial films grown on highly mismatched substrates, such as GaN on sapphire, the epitaxial lateral overgrowth (ELO) technique has been shown to be effective.[7–9] In this technique, epitaxial growth is performed on a seed layer (GaN on sapphire, for example) with a periodically patterned mask on the surface.

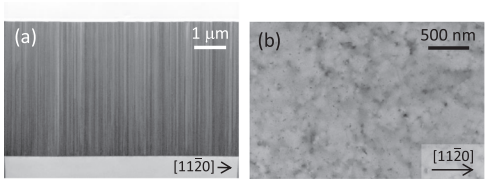

FIG. 1. TEM images of a conventional (0001) α-Ga_2O_3 film grown by HVPE. (a) Cross-sectional image and (b) plan-view image.

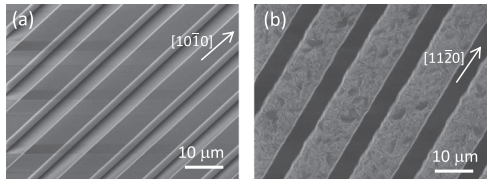

FIG. 2. SEM images of α-Ga_2O_3 stripes grown on an (a) SiO_2 mask and (b) TiO_2 mask (bird's-eye view).

The dimension of the mask width and windows are typically of micro-meter size, and the epitaxial growth begins selectively on the windows to form isolated islands of the target crystal. The islands then grow vertically and laterally and finally coalesce with each other to form a flat film. In this growth process, dislocations in the seed layer under the mask do not propagate into the grown layer. Although dislocations in the seed layer propagate into the grown layer through the windows, the dislocations bend toward the lateral direction to minimize the elastic strain energy if the islands have inclined facets. As a result, the density on the film surface is reduced dramatically. The ELO technique is essential to grow high-quality GaN by heteroepitaxy, and the threading dislocation density reduces typically from 10^9 cm^{-2} to 10^6 cm^{-2} or less.[7–9] The ELO of α-Ga_2O_3 has already been demonstrated.[10] In the demonstration, a stripe-patterned SiO_2 mask with a mask/window size of 2 μm/2 μm was formed directly on a (0001) sapphire substrate, and α-Ga_2O_3 was grown by mist-CVD. Although coalescence was not achieved, cross-sectional TEM revealed that no dislocation propagated into the laterally grown wing region on the mask.

To reduce the dislocation density effectively by ELO, a small mask fill factor, that is, a small window size and wide window spacing, is desirable. However, a smaller fill factor mask requires thicker growth for coalescence, and a fast growth rate is therefore preferable. From this point of view, we employed HVPE to grow α-Ga_2O_3 in this work. HVPE is a type of CVD technique that is characterized by a fast growth rate, and the HVPE of α-Ga_2O_3 has already been demonstrated.[3] In the present work, we demonstrate the ELO of α-Ga_2O_3 by HVPE.

We used an HVPE-grown (0001) α-Ga_2O_3 template (approximately 3-μm-thick) on sapphire as a seed substrate. Periodic masks were formed on the template layer, and α-Ga_2O_3 was regrown by HVPE. The growth temperature of α-Ga_2O_3 is typically as low as 500–600 °C, and the driving force of HVPE growth is higher compared with that of mist-CVD. Therefore, a key issue for successful ELO of α-Ga_2O_3 would be the suppression of undesired nucleation on the mask. From this point of view, we have investigated the mask material, mask design, and HVPE growth conditions.

We investigated SiO_2, Ti, TiO_2, and TiN as mask materials. SiO_2 was deposited by RF sputtering. Ti was deposited by electron beam evaporation. TiN and TiO_2 were produced by nitridation and oxidation of the Ti layer, respectively.

We employed a stripe-patterned mask or dot-patterned mask, which had circle-shaped windows arranged to form a triangular lattice pattern. The masks were fabricated by conventional photolithography using a maskless exposure system. The mask/window widths of the stripe-patterned mask were 5 μm/5 μm. The diameter of the circle windows of the dot-patterned mask was 5 μm. The window spacing of the dot-patterned mask (the distance between mask edges of the nearest windows) was 5–20 μm. A 5-μm-wide dot-patterned mask was used unless otherwise mentioned.

We used a home-made atmospheric horizontal quartz HVPE reactor for this study. GaCl and O_2 were used as the precursors. GaCl was synthesized upstream in the reactor by the chemical reaction between metal Ga (>99.999 99% pure) and HCl gas (>99.999% pure) at 570 °C. The GaCl and O_2 were then injected together with N_2 carrier gas into the growth zone downstream in the reactor to grow α-Ga_2O_3 on the substrate. The growth was carried out at 540 °C with partial pressures of GaCl and O_2 supply to be 1.25×10^{-1} kPa and 1.25 kPa, respectively, unless otherwise specified. The total gas flow rate was fixed to be 8 slm. The growth rate for flat α-Ga_2O_3 films was 12 μm/h under these growth conditions. We used α-Ga_2O_3 templates with approximately 3.4 cm^2 area, and the spacial growth rate variation on the wafer was typically ±1% or less.

The morphologies of the grown crystals were observed by scanning electron microscopy (SEM). The crystal quality was evaluated by X-ray rocking curve (XRC) measurements.

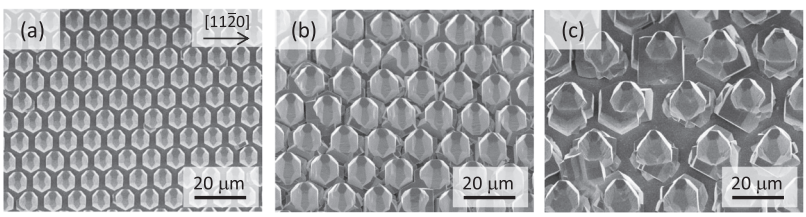

FIG. 3. SEM images of α-Ga_2O_3 islands grown on dot-patterned mask with window spacings of (a) 5 μm, (b) 10 μm, and (c) 20 μm (bird's-eye view).

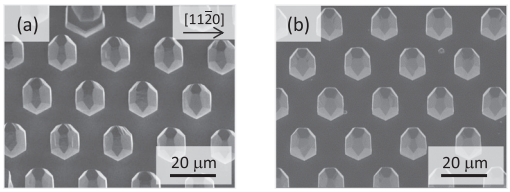

FIG. 4. SEM images of α-Ga_2O_3 islands grown at nominal growth rates of (a) 7 μm/h and (b) 5 μm/h (bird's-eye view).

The behavior of the crystal defects was observed by transmission electron microscopy (TEM).

Figures 2(a) and 2(b) show the SEM images of the samples grown on a SiO_2 mask and a TiO_2 mask, respectively. In the case of the SiO_2 mask, α-Ga_2O_3 stripes grew selectively through the windows, while poly crystal grains nucleated on the TiO_2 mask. This difference was probably not because of the difference of the mask material but because whether the mask was amorphous or crystalline. The results for Ti and TiN masks were similar to those obtained for the TiO_2 mask. We therefore employed an SiO_2 mask in the following experiments.

Figures 3(a)–3(c) show the SEM images of the samples grown for 40 min on the dot-patterned masks with different window spacings of 5, 10, and 20 μm. The same recipe was applied to grow all three samples. When the spacing was 5 μm, we only observed a regular array of α-Ga_2O_3 islands [Fig. 3(a)]. However, when the spacing was wider, extra grains of ε-Ga_2O_3 (not α) nucleated around each α-Ga_2O_3 island [Figs. 3(b) and 3(c)]. In such selective area growth, most of precursors are consumed only at window area. Therefore, the increase in the window spacing (i.e., the decrease in window density) leads to the increase in the effective precursor supply per window. Actually, the island size was larger on the larger spacing mask. Such an increase in the growth driving force would lead to the easier nucleation of the extra grains. Accordingly, a decrease in the precursor supply into the reactor should be effective to suppress the undesired grains. To confirm this, we carried out the growth at slower growth rates. In these growth experiments, only the partial pressure of GaCl supply was decreased from 1.25×10^{-1} kPa to 6.3×10^{-2} kPa and 3.8×10^{-2} kPa. As a result, the nominal growth rate (i.e., the growth rate for flat films) decreased from 12 μm/h to 7 μm/h and 5 μm/h, respectively. A 20-μm-wide dot-patterned mask was used for the growth. Figures 4(a) and 4(b) show the SEM images of the samples. It was found that the nucleation of the extra grains was markedly suppressed under slower growth conditions.

Figures 5(a)–5(c) show the SEM images of the samples grown at 540, 500, and 460 °C. When the growth temperature was 540 °C, the island shape was a hexagonal pillar with a well-developed (0001) plane on the top and small inclined (10$\bar{1}$1) facets. When the temperature was decreased to 500 °C, the (0001) plane became unstable and (10$\bar{1}$1) facets developed well. When the temperature was further decreased to 460 °C, the (0001) plane disappeared and (10$\bar{1}$4) facets appeared instead. As a result, the island shape was dominated by inclined facets. Thus, it was found that the island shape can be controlled by the growth temperature. This feature is useful to carry out facet-controlled ELO.

Figures 6(a)–6(d) show the SEM images of the samples at different growth stages, which are indicated using nominal thickness (i.e., thickness for flat films). At the beginning of the growth, the island shape was similar to that of the circle window [Fig. 6(a)]. Then a hexagonal crystal habit became clear [Fig. 6(b)]. The coalescence process began from the bottom

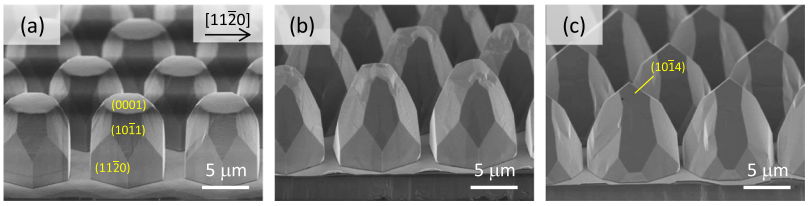

FIG. 5. SEM images of α-Ga_2O_3 islands grown at (a) 540 °C, (b) 500 °C, and (c) 460 °C (bird's-eye view).

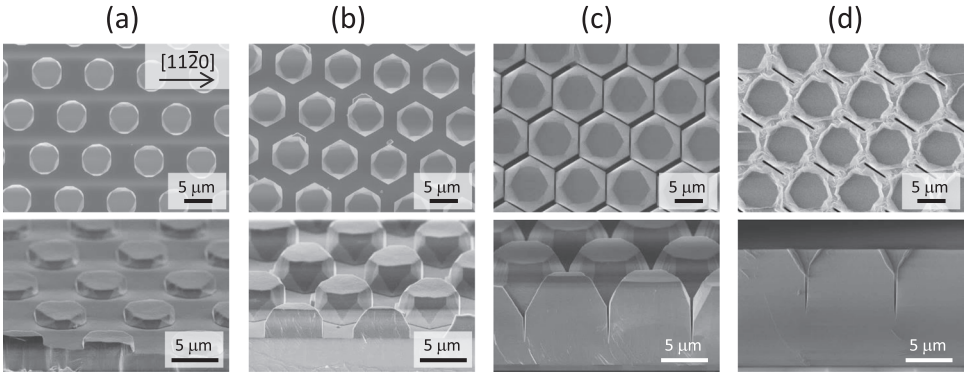

FIG. 6. SEM images of α-Ga_2O_3 islands with nominal thickness of (a) 0.5 μm, (b) 1.6 μm, (c) 8 μm, and (d) 12 μm (plan-view and bird's-eye view).

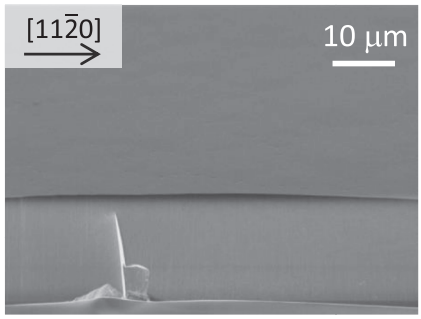

FIG. 7. An SEM image of ELO-grown α-Ga_2O_3 flat film (bird's-eye view).

part of the islands [Fig. 6(c)], and the valley between islands became shallow by continuing the growth [Fig. 6(d)]. Finally, a flat α-Ga_2O_3 film was obtained (Fig. 7).

Figure 8 shows XRC FWHMs of the 0006 and 10$\bar{1}$2 diffraction peaks, measured in symmetric and skew-symmetric geometry, respectively, as a function of the nominal thickness. The FWHM of the 0006 diffraction peak (tilt angle) reflects the tilting of the (0001) plane, while the FWHM of the 10$\bar{1}$2 diffraction peak (twist angle) reflects the twisting around [0001]. It was found that both the tilt and twist angles decreased with increasing nominal thickness, probably owing to the increase in the volume of the high-quality area.

Figure 9 shows the XRC profiles of 0006 and 10$\bar{1}$2 diffractions for the sample with a nominal thickness of 12 μm. In the case of GaN ELO, the XRC profile of the out-of-plane diffraction sometimes show splitting reflecting the formation of small angle grain boundaries because of wing tilting during the lateral growth.[11,12] However, no such splitting was observed in Fig. 9. This result indicated that wing tilting was not significant in the case of ELO-grown α-Ga_2O_3, although the reason for this needs to be clarified in future work.

To clarify the behavior of dislocations in the ELO-grown α-Ga_2O_3, we carried out cross-sectional TEM for a coalesced sample. The growth was carried out at 520 °C for 2 h.

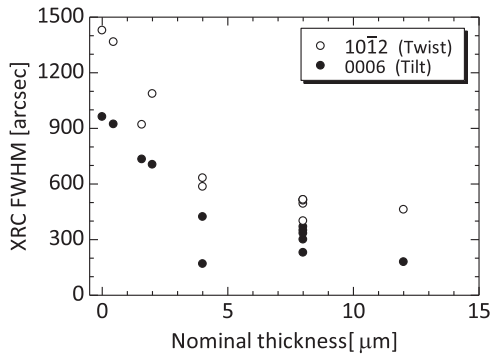

FIG. 8. XRC FWHMs of ELO-grown α-Ga_2O_3 as a function of nominal thickness.

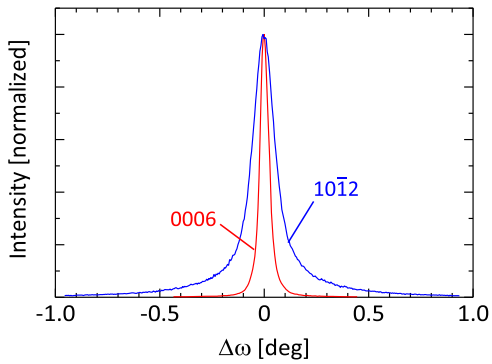

FIG. 9. XRC profiles of ELO-grown α-Ga_2O_3 with a nominal thickness of 12 μm.

(10$\bar{1}$1) inclined facets develop well during the island growth process at this growth temperature. Figure 10(a) shows the plan-view SEM of the sample surface. The surface was still bumpy, and the positions of the windows and coalesced boundaries could easily be identified. Figure 10(b) shows the schematic of the cross section of the sample, and the dotted-line rectangle shows the observation area of the cross sectional TEM. Figure 10(c) shows the TEM image. In the α-Ga_2O_3 template layer under the mask, a high density of dislocations was observed. The dislocations propagated into the regrown layer through the window. Then the dislocation bending started from the vicinity of the mask edge toward the window center successively as the growth proceeded.

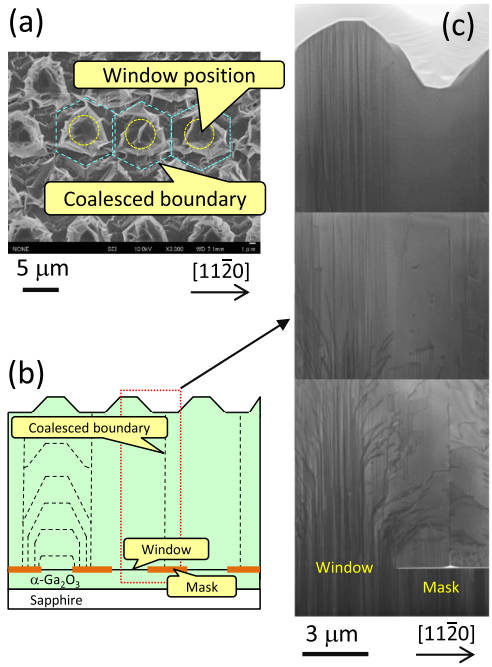

FIG. 10. (a) Plan-view SEM image of a coalesced α-Ga_2O_3 film. (b) Schematic of the cross section. (c) Cross-sectional TEM image of the film.

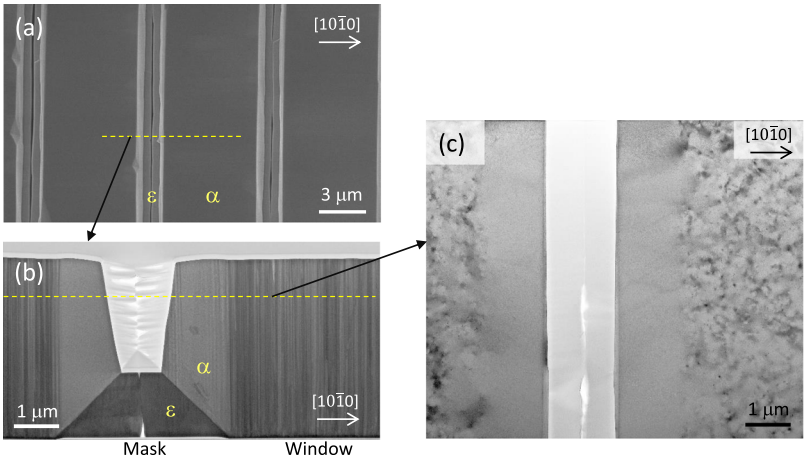

FIG. 11. SEM and TEM images of α-Ga_2O_3 stripes with well-developed (0001) plane. (a) Plan-view SEM image, (b) cross-sectional TEM image, and (c) plan-view TEM image.

As will be described later, such bending was not observed when the inclined facets were not well developed. The dislocation bending therefore probably arose from the inclined facets. We could still see the contrast of crystal defects in the top part above the window, but the density was much lower than that in the template layer. The defect density should be further decreased by controlling the island morphology so that the (0001) plane disappears completely. It is possible that the residual defects include not only dislocations but also other types of crystal defects, such as staking faults. Dark-field observation is now ongoing to identify the types of the defects. At the coalesced boundary just above the mask, we can see dislocation contrasts, which indicated that the crystal orientations of the adjacent islands were not completely the same. The number of dislocations at the boundary decreased with increasing thickness, and no dislocation was found at the top part. The crystal quality should be further improved if we carry out the ELO process twice with positioning the second mask so that the first windows areas are covered. Note that the behavior of dislocations described above might be dependent on the mask direction with respect to the crystal orientation. The mask direction issue is quite important to reduce the dislocation density effectively, and it should be addressed in the future work.

To confirm that the dislocation bending described above can be attributed to the inclined facets, we carried out TEM of a sample which was grown so that the (0001) plane was well developed by raising the growth temperature to 560 °C. A 5-μm-wide stripe-patterned mask was used for the growth. Figure 11(a) shows the plan-view SEM of the sample. Each α-Ga_2O_3 stripe was accompanied by (0001) ε-Ga_2O_3 on both sides. Since lateral growth rate of (0001) ε-Ga_2O_3 is larger than that of (0001) α-Ga_2O_3 under the growth conditions used for this experiment, the ε-Ga_2O_3 parts were about to coalesce with each other, while α-Ga_2O_3 parts were still separated. Figure 11(b) shows a cross-sectional TEM image of the sample. No dislocation bending was found in contrast to the case of the above-mentioned sample grown with well-developed inclined facets. Figure 11(c) shows a plan-view TEM image of the sample. No dislocation was found in the laterally grown areas (approximately 22 μm^2 in total), and therefore, the dislocation density should be less than 5×10^6 cm^{-2} in these areas. Note that it is not clear at present if this dislocation density is sufficiently low or not for power device applications, because it is quite specific to each semiconductor material, and is strongly dependent on the device structure and drive conditions. Further work is required to clarify the influence of crystal defects in α-Ga_2O_3 devices in order to make it clear how low the defect density should be.

We have demonstrated the ELO of α-Ga_2O_3 by HVPE for the first time. Selective area growth was achieved by using SiO_2 as a mask material. Although ε-Ga_2O_3 grains nucleated around each α-Ga_2O_3 island when the window spacing was wide, such extra grains were suppressed by decreasing the precursor supply. It was found that the morphology of α-Ga_2O_3 islands was sensitive to the growth temperature, and inclined facets developed well at low temperatures. XRC measurements showed that both tilt and twist angles decreased with increasing nominal growth thickness, which reflected the increase in the high-quality portion. The out-of-plane XRC did not show peak splitting, which indicated no significant wing tilting and resulting small angle grain boundaries, as can be observed in ELO-grown GaN. Cross-sectional TEM of a coalesced film visualized the dislocation bending, which should be caused by the inclined facets. Such dislocation bending is useful to reduce the dislocation density above the windows. Although some dislocations were observed just above the mask along the coalesced boundary, no dislocation was found in the vicinity of the sample surface. These results show that the ELO technique by HVPE is promising to grow high-quality α-Ga_2O_3, which would lead to the realization of high-performance α-Ga_2O_3 power devices.

Part of this work is based on the results obtained from a project commissioned by the New Energy and Industrial Technology Development Organization (NEDO).

REFERENCES

[1]R. Roy, V. G. Hill, and E. F. Osborn, J. Am. Chem. Soc. **74**, 719 (1952).
[2]D. Shinohara and S. Fujita, Jpn. J. Appl. Phys., Part 1 **47**, 7311 (2008).
[3]Y. Oshima, E. G. Villora, and K. Shimamura, Appl. Phys. Express **8**, 055501 (2015).
[4]M. Oda, R. Tokuda, H. Kambara, T. Tanikawa, T. Sasaki, and T. Hitora, Appl. Phys. Express **9**, 021101 (2016).
[5]K. Kaneko, S. Kan, T. Hitora, and S. Fujita, in The 64th JSAP Spring Meeting, 16p-P8-19, Yokohama, Japan, 2017.
[6]K. Kaneko, S. Fujita, and T. Hitora, Jpn. J. Appl. Phys., Part 2 **57**, 02CB18 (2018).
[7]A. Usui, H. Sunakawa, A. Sakai, and A. A. Yamaguchi, Jpn. J. Appl. Phys., Part 2 **36**, L899 (1997).
[8]Y. Oshima, T. Eri, M. Shibata, H. Sunakawa, K. Kobayashi, T. Ichihashi, and A. Usui, Jpn. J. Appl. Phys., Part 2 **42**, L1 (2003).
[9]K. Motoki, T. Okahisa, N. Matsumoto, M. Matsushima, H. Kimura, H. Kasai, K. Takemoto, K. Uematsu, T. Hirano, M. Nakayama, S. Nakahata, M. Ueno, D. Hara, Y. Kumagai, A. Koukitu, and H. Seki, Jpn. J. Appl. Phys., Part 2 **40**, L140 (2001).
[10]A. Takatsuka, M. Oda, K. Kaneko, S. Fujita, and T. Hitora, in The 62th JSAP Spring Meeting, 13a-P18-12, Hiratsuka, Japan, 2015.
[11]P. Fini, C. Thompson, G. B. Stephenson, J. A. Eastman, M. V. Ramana Murty, O. Auciello, L. Zhao, S. P. Denbaars, and J. S. Speck, Appl. Phys. Lett. **76**, 3893 (2000).
[12]A. Sakai, H. Sunakawa, and A. Usui, Appl. Phys. Lett. **73**, 481 (1998).